3-1-2022

Repeated Jumping with the REBOund: Self-Righting Jumping Robot Leveraging Bistable Origami-Inspired Design

Yuchen Sun

Joanna Wang

Cynthia R. Sung
crsung@seas.upenn.edu

Repeated Jumping with the REBOund: Self-Righting Jumping Robot Leveraging Bistable Origami-Inspired Design

Abstract

Repeated jumping is crucial to the mobility of jumping robots. In this paper, we extend upon the REBOund jumping robot design, an origami-inspired jumping robot that uses the Reconfigurable Expanding Bistable Origami (REBO) pattern as its body. The robot design takes advantage of the pattern's bistability to jump with controllable timing. For jump repeatedly, we also add self-righting legs that utilize a single motor actuation mechanism. We describe a dynamic model that captures the compression of the REBO pattern and the REBOund self-righting process and compared it to the physical robot. Our experiments show that the REBOund is able to successfully self-right and jump repeatedly over tens of jumps.

Supplemental video: https://youtu.be/LoCXcwIxCgU

Keywords

origami robot, jumping

Disciplines

Engineering | Robotics

Repeated Jumping with the REBOund: Self-Righting Jumping Robot Leveraging Bistable Origami-Inspired Design

Yuchen Sun*, Joanna Wang*, Cynthia Sung

***Abstract*— Repeated jumping is crucial to the mobility of jumping robots. In this paper, we extend upon the REBOund jumping robot design, an origami-inspired jumping robot that uses the Reconfigurable Expanding Bistable Origami (REBO) pattern as its body. The robot design takes advantage of the pattern's bistability to jump with controllable timing. For jump repeatedly, we also add self-righting legs that utilize a single motor actuation mechanism. We describe a dynamic model that captures the compression of the REBO pattern and the REBOund self-righting process and compared it to the physical robot. Our experiments show that the REBOund is able to successfully self-right and jump repeatedly over tens of jumps.**

I. Introduction

Jumping is a widely used locomotion strategy for adapting to complex, unstructured environments, overcoming obstacles, and avoiding accidents [1]. The process of jumping involves storing energy and then suddenly releasing it. Controlling the amount of energy stored, contact with the ground, and the landing posture affects the resulting jump height, direction, and the orientation when landing [2], [3].

Jumping robots use a wide variety of energy storage and actuation strategies. Linkage mechanisms and torsional springs are common in miniature jumping robots. Rapid release is achieved through latching mechanisms: tendons [4], [5], drop cams [6], or sliding windows [7]. Jumping robots such as Salto-1P [8] and Tailbot [9], which aim at adjusting aerial posture, used a spring-pendulum mechanism as the main body. To reduce the weight of the body, most of the robots are optimized to use as few actuators as possible. The omnidirectional jumper [10] is designed to use only 2 motors: one for accumulating energy and self-righting, one for steering and take-off angle adjustment. TAUB [11] further reduced the number of actuators to one, which could individually control self-righting after landing and reorientation of jumping. Additional strategies include embedding SMA springs [12], [13] or DEAs [14] to further reduce the weight of the jumper and maximize jump height.

In previous work, we introduced the origami-inspired REBOund jumper [15]. Unlike the above jumping robots, which typically use springs for energy storage, the REBOund has been developed to make the full use of the fold pattern itself. REBOund is constructed from the Reconfigurable Expanding Bistable Origami (REBO) [16], a non-rigidly foldable origami pattern that simultaneously serves as frame and jumping mechanism. By tuning the parameters of the origami pattern, the strain energy stored in the pattern can be manipulated, and thus the control strategy for jumping is relatively simple. Due to the simplicity of the actuation strategy, however, the original REBOund robot was unable to control its takeoff and landing behavior, making it difficult to jump repeatedly. The design used four passive latching mechanisms that required precise synchronization, making it difficult to control the timing and orientation of takeoff. Further since the design was top-heavy, it usually landed on its side, making repeated jumping impossible.

In this paper, we introduce a new design that addresses both of these issues, resulting in a lightweight origami-inspired jumper with the capacity for repeated jumping. In order to control jump timing, we redesign the REBOund body to be bistable, allowing it to remain at its compressed (high spring energy) state indefinitely until triggered to jump. The concept is similar in nature to jumpers such as [17], [18], but our design incorporates sensors and control electronics and is completely untethered. For self-righting, we take inspiration from mechanisms in [4], [10] and add legs to the outside of the robot allowing it to push itself upright. The contributions of this paper include:

- an extension to the REBOund origami-inspired jumping robot that performs repeated jumping by self-righting;
- an experimentally-verified pseudo-rigid-body model that incorporates self-contact of the fold pattern;
- a dynamical model of REBOund self-righting; and
- demonstrations of the REBOund robot with different design parameters for self-righting and the ability to perform repeated jumping.

This paper is organized as follows: Section II provides an overview of the robot design and actuation mechanism. Section III describes the self-righting mechanism. Section IV provides a dynamical model for the robot's jumping and self-righting behavior. Section V contains experimental results comparing the model to our physical device. Section VI concludes with a discussion of limitations and future work.

II. Design Overview

The Reconfigurable Expanding Bistable Origami (REBO) pattern is an origami tessellation of repeating vertical and slanted folds that meet at a horizontal fold in the middle, as pictured in Fig. 1 [16]. The flat pattern folds into the shape of two joined frustra, and the parameters of the folded state are

*equal contribution. Y. Sun, J. Wang, and C. Sung are with the General Robotics, Automation, Sensing & Perception (GRASP) Lab at the University of Pennsylvania, Philadelphia, PA, USA. {yuchens, jwang4, crsung}@seas.upenn.edu. Support for this project has been provided in part by NSF Grant No. 1845339 and the Penn Rachleff Scholars program. The authors also thank Peter Szczesniak and Joseph Valdez for their assistance with fabricating the screw drive mechanism, and Shaun Fedrick and Jason Friedman for helpful discussions.

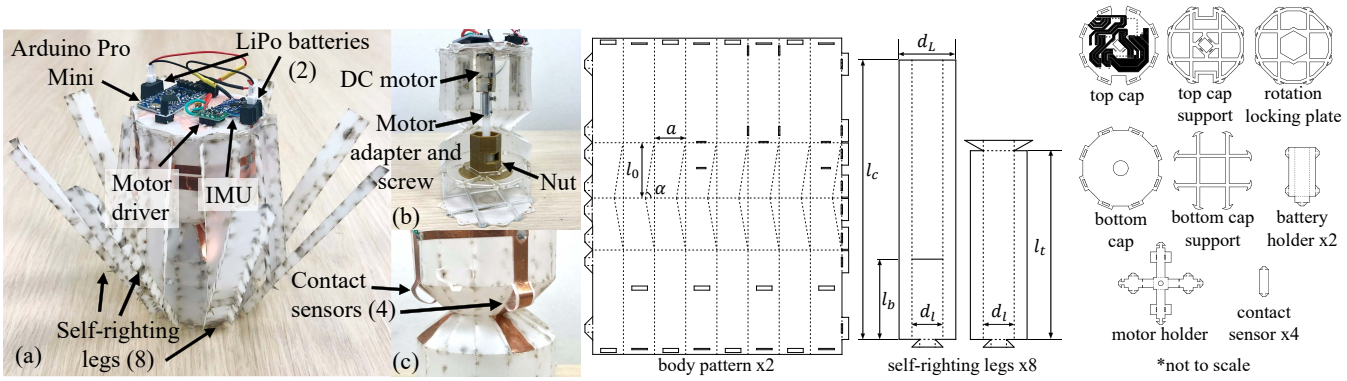

Fig. 1. Left: Final fabricated REBOund design. (a) Assembled robot with self righting legs attached. (b) Internal screw drive mechanism. (c) Close-up of contact sensors. Middle: Main origami components with relevant parameters labeled. Right: Additional laser cut parts (not to scale).

dictated by those of the flat state. When the REBO pattern is compressed heightwise, the two frustra deform, with one folding into the other (ref. Fig 2). Changing the fold pattern parameters alters the behavior of the folded state, e.g., the amount of force required to compress and the stability of the compressed state. In the previous work [15], we designed the compressed state to be unstable, thereby using the pattern as regular spring-like energy storage. In this extension, we re-designed the fold pattern to be bistable (with stable expanded and compressed states) so that we could control jump timing. To tune the design parameters, we focus on the angle of the diagonal fold α, the width of the REBO panel a, and the width of the panel overlap b. As found in [15], increasing α usually leads to an increased jump height but also increases the amount of force required to compress the REBOund. Decreasing b and a so that $a - b$ is constant gives a wider range of parameters α and l_0 that result in a bistable REBO.

We choose parameter values $a = 12$ mm and $b = 0$ mm to achieve bistability in the REBO pattern and decrease l_0 to 20 mm to increase the inner radius. The pattern was cut and folded from 0.127 mm thick PET film and tested experimentally. With these parameter values, patterns with α angles of 79°, 80°, and 81° were foldable and bistable. Of these patterns, $\alpha = 80°$ produces the highest jump while still able to be compressed with our DC motor. Since the pattern is symmetric, it is possible for the frustra to compress in two ways: the bottom folds into the top, or the top folds into the bottom. A slightly higher α value on the top ensures that the top always folds into the bottom. We therefore choose $\alpha_{\text{top}} = 81°$ and $\alpha_{\text{bottom}} = 80°$ for our robot design.

Figure 1 shows the resulting robot and components. The design was fabricated as follows. The main body of the REBOund, including top and bottom caps, motor holder, battery holders, and self righting legs (Sec. III) are cut from 0.127 mm thick PET film on a PLS4.75 laser cutter. Creases are perforated at 35 pulses per inch. Rigid plates laser-cut from 1/16" thick acrylic in the bottom half of the REBOund provide rigidity for the actuation mechanism (Sec. II-A). An additional plate laser-cut from 1/16" PETG is attached to the top cap to support the circuitry.

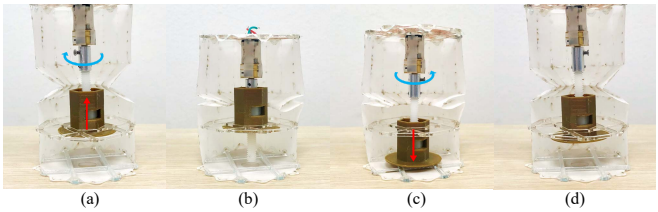

Fig. 2. Screw-drive actuation mechanism. During compression (a-b), the motor pulls the nut up to force the robot into its compressed stable state. To jump (c-b), the motor turns clockwise, pushing the bottom of the pattern until it snaps through to its expanded state and jumps.

A. Actuation

The REBOund employs a screw-drive mechanism consisting of a DC motor (Pololu #3072) connected to a 1/4"-20 nylon threaded rod. This rod interfaces with a 1/4"-20 nylon hex nut embedded inside a 3D printed hexagonal housing The housing fits through a hexagonal cutout in middle 1/16" acrylic plate, which restricts the housing rotation, converting the motor's rotational motion into purely linear motion.

The jump sequence consists of a compression and decompression phase. During the compression phase, the motor rotates counter-clockwise to move the housing upward (Fig. 2(a)). When the flange of the housing comes into contact with the middle plate, the top half of the REBOund is pulled downward until it reaches its fully compressed stable state (Fig. 2(b)). During expansion, the motor rotates in the reverse direction to push the housing down Fig. 2(c). Due to the REBOund's bistability, it stays in its compressed state while the housing travels. When the housing flange hits the bottom of the robot, it exerts a force pushing the top and bottom of the REBOund apart. Once the REBOund is pulled past its unstable equilibrium, it snaps to its expanded state (unconstrained by the motor) and jumps. (Fig. 2(d)).

B. Sensing and Electronics

Control electronics are mounted on the top of the robot. Circuit traces cut out of copper foil tape using a Cameo Silhouette are adhered onto the top face before cutting the pattern. The actuation system is controlled using an Arduino Pro Mini and DRV8838 motor driver.

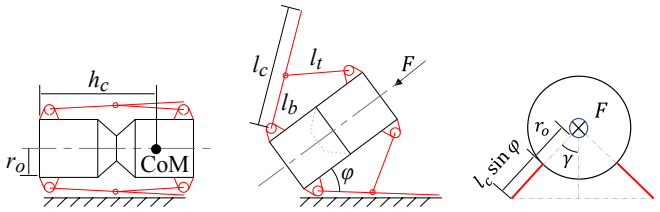

Fig. 3. Self-righting mechanism. The legs are composed of two links that push the robot upright. The leg angle φ is the angle between the leg and the ground. Tipping occurs when φ exceeds a critical angle φ_c. Left: extended state. Middle: compressed state. Right: Compressed state observed from F.

The robot tracks its state (orientation, angular velocity) using a GY-521 MPU-6050 three-axis accelerometer. To track the REBOund's posture and compensate for drift, the IMU readings are processed using a complementary filter at with a frequency of 100 Hz. Additionally, four contact sensors made of copper foil tape and 0.127 mm PET are situated around the center of the REBOund to detect when the REBOund is fully compressed.

Compression of the REBOund begins in response to a button press or when it is tipped over and ends when the contact sensors trigger. After a delay to allow for self righting, the REBOund begins its decompression cycle. After the contact sensors lose contact, the motor continues to spin for 300 ms and the REBOund jumps.

III. Self-Righting Mechanism

Self-righting is achieved via legs attached to the top and bottom edges of the robot (Fig. 3). The bottom leg l_b is the longer of the two and is responsible for pushing the robot upright. The top leg l_t connects the bottom leg to the top of the robot so that the angle of the bottom leg changes when the robot compresses. When the REBOund is in the expanded state, the bottom leg is oriented at an angle φ from the center axis of the robot. As the REBOund compresses, the legs rotate outwards, increasing φ. If the REBOund is on the ground, this rotation generates a reaction force to push the REBOund upright. The fold pattern of the self-righting mechanism is shown in Fig. 1. The legs consist of two separate rectangular pieces connected at the ends to the REBO and at the center to each other. The rectangular tabs on the sides of the legs increase stiffness.

This maneuver will succeed as long as the robot's center of mass is pushed over the corner. Let r_o be the radius of the body and h_c be the height of the center of mass of the robot off the ground. We assume the robot is rotationally symmetric so that the center of the mass is lying on the centerline of the REBOund and the model can be simplified to a planar model. Let θ be the angle between the robot's body and the ground. Then the robot will self-right if

$$\tan(\theta) > \tan(\theta_c) = \frac{h_c}{r_o} \tag{1}$$

The lengths l_t and l_b should be chosen so that the angle of the legs φ is able to achieve this condition. The relationship between l_t, l_b, and φ is shown via the law of cosines as

$$2hl_b \cos\varphi = l_b^2 + h^2 - l_t^2 \tag{2}$$

where h is the total height of the REBOund.

If the entire robot is completely surrounded by legs, then $\varphi = \theta$, and we can solve for the necessary leg lengths. However, if φ is able to exceed the critical angle θ_c in Eq. (1), then it is possible to reduce the number of legs without losing self-righting capabilities. Given leg dimensions, if the maximum achievable angle is $\varphi_{\max}$, then legs must be spaced at least an angle $\gamma_{\min}$ apart according to

$$\tan\theta_c = \frac{(r_o + l_c \sin\varphi_{\max})\cos(\gamma_{\min}/2)}{l_c \cos\varphi_{\max}} \tag{3}$$

which characterizes the angle of the robot relative to the ground when it lands precisely with two legs on the ground. The minimum number of legs that can be used is then

$$N_{min} = \left\lceil \frac{2\pi}{\gamma_{\min}} \right\rceil \tag{4}$$

IV. Dynamical Model of REBOund Self-Righting

In this section, we introduce our dynamical self-righting model. In order to compute the dynamics of the robot, we first analyze the mechanics of the REBOund body and the compressive force produced by the motor, then combine it into our full dynamical model.

A. Fold Pattern Mechanics

The behavior of the REBO pattern can be predicted using a pseudo-rigid body model where the REBO is simplified into a trapezoidal arrangement of springs as shown in Fig. 4 [15]. The vertical spring force F_S produced by the REBO when it is compressed is

$$F_S = F_\beta + F_d \tag{5}$$

$$F_\beta = \frac{k_\beta}{l_\gamma}(\beta - \beta_0)\sec\beta \tag{6}$$

$$F_d = -4k_d l_\gamma (\cos\beta - \cos\beta_0)\tan\beta \tag{7}$$

where k_β and k_d are torsional and linear spring constants, respectively, β is the slant angle of the frustrum in the REBO, β_0 is the rest angle of the fully expanded REBO, and l_γ is the effective length of the slanted faces in the fold pattern. The angle β and the REBOund height h are coupled as

$$h = h_{\min} + l_\gamma \sin\beta \tag{8}$$

In addition, when the pattern is highly compressed, the faces of the pattern come into contact and generate additional forces that prevent self-intersection. We model this force using a barrier function

$$F_c = \begin{cases} \frac{\eta}{(\beta_0+\beta)^\zeta} + C & \beta < \beta_c \\ 0 & \beta \geq \beta_c \end{cases} \tag{9}$$

In this expression, $\beta_0+\beta$ is the angle between the two slanted faces in the middle of the REBO pattern, and η is the strength of the collision force (determined by the material properties and the pattern geometry). The parameter C is calculated

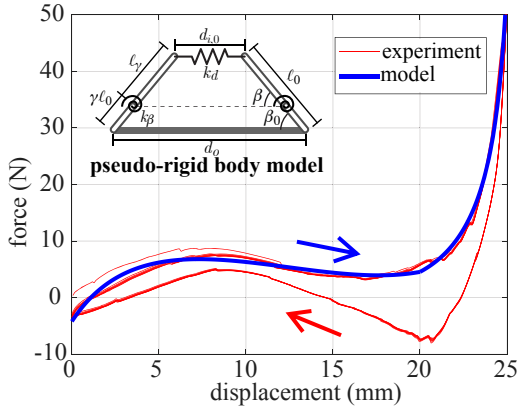

Fig. 4. All 8 trials of measured force vs. displacement for REBO pattern, along with the predicted force-displacement curve. Red lines are the measured values from MTS machine. Positive values indicate compressive force while the negative values indicate tension force. Blue arrows: compression. Red arrows: tension.

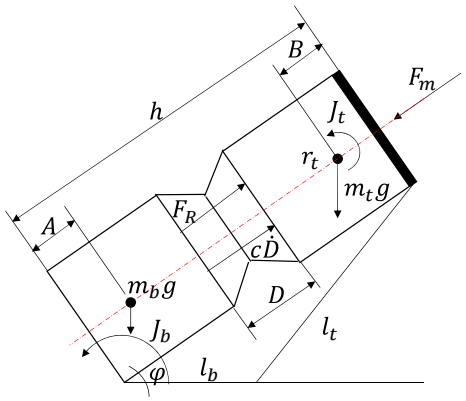

Fig. 5. Sagittal plane diagram of REBOund parameters, where A is the distance from bottom to bottom C.o.M, B is the distance from top to top C.o.M, J_t is top part's moment of inertia w.r.t its C.o.M, and J_b is the bottom part's moment of inertia w.r.t the pivot. D is the compression distance

such that F_c is continuous at the critical angle $\beta = \beta_c$. The collision force F_c starts when the REBO is not in self-contact ($\beta < \beta_c$) and increases to infinity as the angle between faces goes to 0 ($\beta \to -\beta_0$). Then the total vertical force required to compress the REBO is

$$F_R = F_S + F_c = F_\beta + F_d + F_c \tag{10}$$

Figure 4 shows a comparison of this new model to compression tests taken on an MTS Criterion Model C41 testing machine with 1 kN load cell. The REBO was compressed and extended 8 times. The sample is physically bistable, as indicated by the tension curve with 2 stable equilibria. Hysteresis was also observed in each cycle, indicating some energy loss in the pattern, likely because the deformation for compression and tension are not the same. During compression, we observed that both sides of the REBO pattern bent, whereas during tension, only the bottom face bent.

Since we are interested in the robot's self-righting behavior, we fit our model to the compression curve. As seen in the plot, the new model accurately captures the rise in compressive force required when the compression amount exceeds 20 mm. This curve was used to determine the actuation requirements for the robot.

B. Motor Compressive Force

The REBOund is compressed by a motor force F_m. Based on standard motor torque-speed relationships, the output torque of the motor τ_m and the speed ω_m are related by

$$\omega_m = \omega_0 - k_\tau \tau_m \tag{11}$$

where ω_0 is the no-load speed of the motor and k_τ is the motor constant. The screw drive mechanism increases the output torque by an effective gear ratio χ_m. Thus

$$F_m = \chi_m \tau_m \tag{12}$$

$$\dot{h} = \omega_m / \chi_m \tag{13}$$

Practically, the gear ratio χ_m can be computed as

$$\chi_m = 2\pi / p \tag{14}$$

where p is the thread pitch.

C. Self-Righting of the REBOund

To model self-righing of the REBOund, we analyze a planar dynamical model, assuming that the robot is perfectly rotationally symmetric and ignoring 3D rotations (Fig. 5).

When the robot is moving, the kinetic energy T and potential energy P for the whole system are written as

$$T = \frac{1}{2} m_t \dot{r}_t^2 + \frac{1}{2} J_t \dot{\theta}^2 + \frac{1}{2} J_b \dot{\theta}^2 \tag{15}$$

$$P = m_b g y_b + m_t g y_t + U \tag{16}$$

where r_t is the position of the top C.o.M, θ is the angle between the robot's body and the ground. We treat the top and bottom of the robot as separate rigid bodies since they move relative to each other when the REBOund compresses. In addition, m_t and J_t are the mass and moment of inertia about the center of mass (CoM) of the top, respectively, J_b is the moment of inertia of the bottom about the pivot point, and U is the strain potential energy stored in the REBO body. The Lagrangian for the system is

$$L = T - P \tag{17}$$

Before the REBOund reaches the critical state, h and θ are coupled. In particular, the leg is in contact with the ground, so the tilt of the robot θ is equal to the leg angle φ, and the leg angle is constrained by the height of the robot according to Eq. (2) (or Eq. (3) if fewer legs are used). Thus, we can write the equation of motion of the system as

$$\frac{d}{dt}\left(\frac{\partial L}{\partial \dot{q}_j}\right) - \frac{\partial L}{\partial q_j} + \sum_{r=1}^{m} \lambda_r \frac{\partial f}{\partial q_j} = \sigma_j \tag{18}$$

where $q = [h, \theta]$ and σ is the general force

$$\sigma_1 = F_R - F_m - c\dot{h} \tag{19}$$

$$\sigma_2 = 0 \tag{20}$$

TABLE I

MASS BREAKDOWN

REBOund component	Mass (g)
fold pattern	5.5
self-righting legs (8x)	6.2
support plates	5.1
batteries (2x)	8.2
motor and screw-drive mechanism	15.5
electronics	9.8
Total	50.3

TABLE II

FINAL DESIGN PARAMETERS

Pattern Geometry					
α_{bottom}	=	80°	α_{top}	=	81°
N	=	16	a	=	12 mm
r_o	=	30.1 mm	b	=	0 mm
l_0	=	20 mm	$h_{\max}$	=	110 mm
$h_{\min}$	=	80 mm			
Pattern Mechanics					
k_β	=	135.3	k_d	=	0.8
η	=	1.9	ζ	=	1.2
β_0	=	0.7 rad	c	=	8.0 N·s/mm
Actuation Parameters					
ω_0	=	129.1 rad/s	k_τ	=	180
χ_m	=	4.94			
Additional Robot Parameters					
m_t	=	45.3 g	m_b	=	7.9 g
h_c	=	65.3 mm	ϕ_c	=	65°

where F_m is the compression force exerted by the motor, c is a damping coefficient, and $\partial f/\partial q_j$ is the constraint between h and θ such that

$$\frac{\partial f}{\partial h} = 2h - 2l_b \cos\varphi \tag{21}$$

$$\frac{\partial f}{\partial \theta} = 2hl_b \sin\varphi \tag{22}$$

Note that h, y_t, and y_b are related linearly.

After the REBOund reaches the critical state, the bottom leg will no longer push against the ground and the REBOund will stand up under gravity. In this case, h and θ are independent variables so we may simply use

$$\frac{\partial f}{\partial h} = \frac{\partial f}{\partial \theta} = 0 \tag{23}$$

V. EXPERIMENTAL RESULTS

The new REBOund design with revised actuation mechanism was constructed as pictured in Fig. 1. The final parameters in the design are shown in Table II.

A. Jumping via Bistable Body

We first tested the robot without self-righting legs. The fabricated REBOund robot was placed on flat ground, and its jumping behavior was recorded at 240 fps to track the motion of the center of the robot. The robot is able to successfully compress and jump. When actuated by hand such that there is no weight on the pattern other than the pattern itself, the designed pattern jumps 220 mm, which is higher than the previous highest-jumping REBOund from [15] achieving a maximum height of 167.4 mm. However, when electronically actuated and controlled, the new REBOund jumps at a lower height (75.0 mm) than the old one (123.4 mm) even accounting for the increased weight (ref. Table IV). We believe some energy is lost by snapping through to the compressed bistable state. This trade-off in jump height was acceptable to enable repeatable jumping, which is required for future functions.

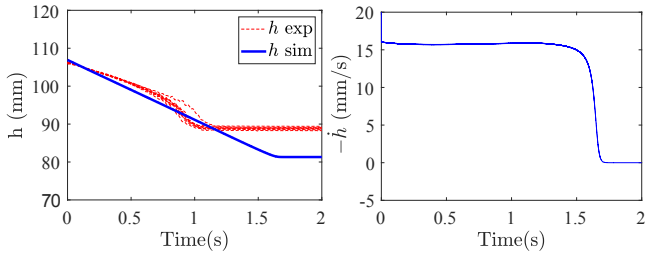

Fig. 6. Left: Simulated vs experimental h over time. Right: Simulated $-\dot{h}$ over time. Solid and dashed curves indicate simulation and experiment data respectively.

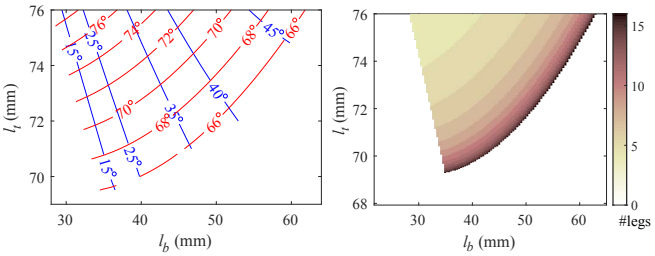

Fig. 7. Left: Contour plot of $\varphi_{\min}$ and $\varphi_{\max}$ over leg length parameters. Blue lines: $\varphi_{\min}$, Red lines: $\varphi_{\max}$. Right: smallest number of legs required for self-righting.

Full compression requires about 1.2 s, which is less than the 1.7 s predicted by simulation (Fig. 6), and the REBO compresses less than expected. This is likely because friction in the motor, combined with contact forces in the REBO, cause the pattern not to fully compress. We experimentally determined that it is not necessary to compress the REBOund to full compression for it to snap into its compressed state. Practically, in order to prevent stalling and motor burnout, we thus designed the contact sensors to trigger once the REBOund had compressed by 17 mm. In order to jump, the motor must fully reverse and pop the REBOund in the upward direction. This process took 1.14 s on average.

B. Self-Righting

We also tested the design's ability to self-right. Based on the analysis in Section III, we computed the space of feasible l_t and l_b values. As shown in Fig. 7, larger values of $\varphi_{\max}$ occur for larger values of l_t and smaller values of l_b. At the same time, it is desirable to keep $\varphi_{\min}$ small so that the legs fit compactly against the REBOund surface when jumping to minimize drag. These smaller $\varphi_{\min}$ values occur for smaller l_b values. The optimal leg is theoretically (l_b, l_t) in the upper left corner. In addition, with these parameters, only 4 legs are theoretically required for the REBOund to self-right.

To test the accuracy of these predictions, we tested REBOunds with legs of different parameters. Table III shows the

TABLE III

SELF-RIGHTING PERFORMANCE ON DIFFERENCE LEG LENGTH

(l_b, l_t) (mm)	$\varphi_{\min}$	$\varphi_{\max}$	Success	Time to Right (s)
$(28, 76)$	0	80°	Yes	1.40
$(31, 73)$	0	72°	Yes	1.30
$(34, 70)$	0	66°	No	/

TABLE IV

SELF-RIGHTING PERFORMANCE ON $(l_b, l_t) = (28, 76)$

Leg number	Success	Right Time (s)	Jump height (mm)
16	Yes	1.25	35.8 ± 1.7
8	Yes	1.40	51.5 ± 3.2
4	No	/	54.3 ± 1.4
0	No	/	75.0 ± 2.9

Jump height shown as mean $\pm$ 1 standard deviation

parameters tested and the results. All tests were completed using 8 legs. Note that legs are inserted to the slots some distance away from top and bottom edge, so $h_{\max} = 104$ mm in simulation. Both the $(l_b, l_t) = (28, 76)$ mm and the $(l_b, l_t) = (31, 73)$ mm legs are predicted to be able to self-right with 8 legs and are able to do so successfully. The $(l_b, l_t) = (34, 70)$ mm legs are predicted to be able to right the REBOund when 8 legs are used, but experimentally, it failed. Compared to the theoretical assumptions that the legs remained rigid, the physical legs bend during self-righting and are unable to push past the critical θ.

We then tested varying the number of legs with the optimal leg dimensions $(l_b, l_t) = (28, 76)$ mm. The robot was laid on its side on flat ground and commanded to self-right then jump in sequence. For robots that did not successfully self-right, we also tested the jump height separately. Results are shown in Table IV. The REBOund is able to successfully right itself with 8 and 16 legs. The robot is predicted to be able to right itself with 4 legs, but does not succeed in experiments, again, likely due to leg compliance.

Figure 8 shows the experimentally measured tilt angle θ and the angles of the legs off the ground $\theta - \varphi$ over time. When the REBOund is on the floor ($\theta = 0$), the legs bend under the weight of the robot and have a harder time pushing the robot upwards, so the tilt angle is lower in experiments than predicted by simulation. Once the robot moves to be oriented more upright, the forces on the legs become smaller and the legs converge back to the expected angles by the time the robot hits the critical tilt. After the REBOund reaches the critical state, the self-righting legs leave the ground and the REBOund self-rights under gravity. For both sets of tested parameters, the REBOund reaches the upright position before it snaps into the fully compressed state. We compared the predicted self-righting time from the simulation to the experiments. For $(l_b, l_t) = (28, 76)$ mm, it takes 1.18 s to reach upright position in simulation, while it takes 1.09 s to fully compress in experiments and 1.40 s to be fully upright. For $(l_b, l_t) = (31, 73)$, it takes 1.37 s to reach upright position in simulation, while it takes 1.17 s to compress in experiment and 1.30 s to be fully upright. The reason for this is that we assume the REBOund is 2D

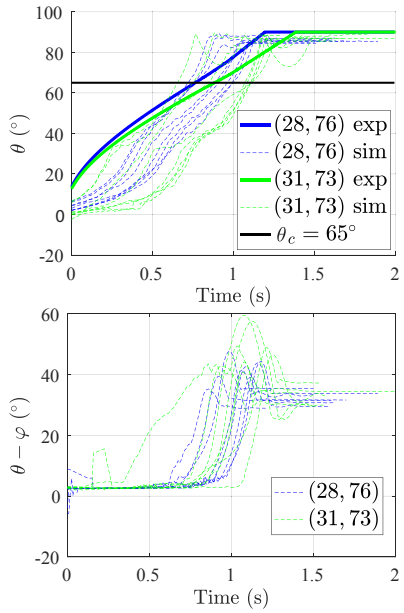

Fig. 8. Top: θ over time for $(l_b, l_t) = (28, 76), (31, 73)$. Solid and dashed curves indicate simulation and experiment data. Bottom: Angle between the bottom leg and the ground over time.

in simulation, but practically the robot tends to roll out of plane before settling into its final upright state.

C. Repeated Jumping

Finally, the REBOund was commanded to jump repeatedly on a flat surface to test reliability. In one trial, the REBOund jumped 13 times (self-righting twice) continuously. Over 77 total jumps, it fell over on 42.8% jumps and successfully self-righted in each case. The average time for compression when not self-righting was 0.93 s, and the average time for self-righting was 1.19 s.

VI. DISCUSSION

In this paper, we present a self-righting bistable design for the REBOund jumping robot. The REBOund is a 50.3 g origami-inspired robot that leverages a bistable origami pattern for its body to jump up to 70.5 mm. We also present a model and experimental results for leg attachments allowing the robot to self-right upon falling and to jump repeatedly.

Future work includes further investigation into the loss of jump height after reaching the compressed stable state, and if the actuation or body material can be optimized to minimize energy loss. Additionally, the weight of the REBOund can be reduced to increase jump height. Another direction of future work is directional jumping and multimodal locomotion. These functions are required for the robot to be able to navigate complex terrain in the future. For example, although the robot is theoretically rotationally symmetric, an assymmetric mass distribution causes it to roll during self-righting. This is not desired for self-righting but does create new opportunities for rolling locomotion or steering in preparation for sideways jumps in the future. We will need to expand our dynamical model to 3D to take advantage of this motion.

REFERENCES

[1] X. Mo, W. Ge, M. Miraglia, F. Inglese, D. Zhao, C. Stefanini, and D. Romano, "Jumping locomotion strategies: From animals to bioinspired robots," *Applied Sciences*, vol. 10, no. 23, p. 8607, 2020.

[2] L. Zhang, H. Chen, and Y. Yang, "Review on mechanism and modeling of jumping robot," in *IEEE International Conference on Cyber Technology in Automation, Control, and Intelligent Systems*, 2016, pp. 255–260.

[3] C. Zhang, W. Zou, L. Ma, and Z. Wang, "Biologically inspired jumping robots: A comprehensive review," *Robotics and Autonomous Systems*, vol. 124, p. 103362, 2020.

[4] J. Zhao, J. Xu, B. Gao, N. Xi, F. J. Cintron, M. W. Mutka, and L. Xiao, "MSU jumper: A single-motor-actuated miniature steerable jumping robot," *IEEE Transactions on Robotics*, vol. 29, no. 3, pp. 602–614, 2013.

[5] V. Zaitsev, O. Gvirsman, U. B. Hanan, A. Weiss, A. Ayali, and G. Kosa, "A locust-inspired miniature jumping robot," *Bioinspiration & Biomimetics*, vol. 10, no. 6, p. 066012, 2015.

[6] M. Kovac, M. Fuchs, A. Guignard, J.-C. Zufferey, and D. Floreano, "A miniature 7g jumping robot," in *IEEE International Conference on Robotics and Automation (ICRA)*, 2008, pp. 373–378.

[7] S. Li and D. Rus, "Jellocube: A continuously jumping robot with soft body," *IEEE/ASME Transactions on Mechatronics*, vol. 24, no. 2, pp. 447–458, 2019.

[8] J. K. Yim and R. S. Fearing, "Precision jumping limits from flight-phase control in salto-1p," in *IEEE/RSJ International Conference on Intelligent Robots and Systems*, 2018, pp. 2229–2236.

[9] J. Zhao, T. Zhao, N. Xi, M. W. Mutka, and L. Xiao, "MSU Tailbot: Controlling aerial maneuver of a miniature-tailed jumping robot," *IEEE/ASME Transactions on Mechatronics*, vol. 20, no. 6, pp. 2903–2914, 2015.

[10] S. Yim, S.-M. Baek, G.-P. Jung, and K.-J. Cho, "An omnidirectional jumper with expanded movability via steering, self-righting and take-off angle adjustment," in *IEEE/RSJ International Conference on Intelligent Robots and Systems*, 2018, pp. 416–421.

[11] A. Weiss, V. Zaitsev, N. Nabi, and U. B. Hanan, "Landing recovery and orientation control of a locust-inspired miniature jumping robot," *Engineering Research Express*, vol. 2, no. 1, p. 015017, 2020.

[12] M. Noh, S.-W. Kim, Sungmin, J.-S. Koh, and K.-J. Cho, "Flea-inspired catapult mechanism for miniature jumping robots," *IEEE Transactions on Robotics*, vol. 28, no. 5, pp. 1007–1018, 2012.

[13] Z. Zhakypov, C. H. Belke, and J. Paik, "Tribot: A deployable, self-righting and multi-locomotive origami robot," in *IEEE/RSJ International Conference on Intelligent Robots and Systems*, 2017, pp. 5580–5586.

[14] M. Duduta, F. Berlinger, R. Nagpal, D. R. Clarke, R. J. Wood, and F. Z. Temel, "Tunable multi-modal locomotion in soft dielectric elastomer robots," *IEEE Robotics and Automation Letters*, vol. 5, no. 3, pp. 3868–3875, 2020.

[15] J. Carlson, J. Friedman, C. Kim, and C. Sung, "REBOund: Untethered origami jumping robot with controllable jump height," in *IEEE International Conference on Robotics and Automation*, 2020.

[16] H. Yuan, J. Pikul, and C. Sung, "Programmable 3-D surfaces using origami tessellations," in *7th International Meeting on Origami in Science, Mathematics, and Education*, 2018, pp. 893–906.

[17] S.-P. Jung, G.-P. Jung, J.-S. Koh, D.-Y. Lee, and K.-J. Cho, "Fabrication of composite and sheet metal laminated bistable jumping mechanism," *Journal of Mechanisms and Robotics*, vol. 7, no. 2, p. 021010, 2015.

[18] S. Nishikawa, Y. Arai, R. Niiyama, and Y. Kuniyoshi, "Coordinated use of structure-integrated bistable actuation modules for agile locomotion," *IEEE Robotics and Automation Letters*, vol. 3, no. 2, pp. 1018–1024, 2018.